MAJOR PAPER

Clinical Application of MPRAGE Wave Controlled Aliasing in Parallel Imaging (Wave-CAIPI): A Comparative Study with MPRAGE GRAPPA

Azusa Sakurama[1], Yasutaka Fushimi[1]*, Satoshi Nakajima[1], Akihiko Sakata[1],
Takuya Hinoda[1], Sonoko Oshima[1], Sayo Otani[1], Krishna Pandu Wicaksono[1],
Wei Liu[2], Takakuni Maki[3], Tomohisa Okada[4], Ryosuke Takahashi[3],
and Yuji Nakamoto[1]

Purpose: To compare reliability and elucidate clinical application of magnetization-prepared rapid gradient-echo (MPRAGE) with 9-fold acceleration by using wave-controlled aliasing in parallel imaging (Wave-CAIPI 3 × 3) in comparison to conventional MPRAGE accelerated by using generalized autocalibrating partially parallel acquisition (GRAPPA) 2 × 1.

Methods: A total of 26 healthy volunteers and 33 patients were included in this study. Subjects were scanned with two MPRAGEs, GRAPPA 2 × 1 and Wave-CAIPI 3 × 3 acquired in 5 min 21 s and 1 min 42 s, respectively, on a 3T MR scanner. Healthy volunteers underwent additional two MPRAGEs (CAIPI 3 × 3 and GRAPPA 3 × 3). The image quality of the four MPRAGEs was visually evaluated with a 5-point scale in healthy volunteers, and the SNR of four MPRAGEs was also calculated by measuring the phantom 10 times with each MPRAGE. Based on the results of the visual evaluation, voxel-based morphometry (VBM) analyses, including subfield analysis, were performed only for GRAPPA 2 × 1 and Wave-CAIPI 3 × 3. Correlation of segmentation results between GRAPPA 2 × 1 and Wave-CAIPI 3 × 3 was assessed.

Results: In visual evaluations, scores for MPRAGE GRAPPA 2 × 1 (mean rank: 4.00) were significantly better than those for Wave-CAIPI 3 × 3 (mean rank: 3.00), CAIPI 3 × 3 (mean rank: 1.83), and GRAPPA 3 × 3 (mean rank: 1.17), and scores for Wave-CAIPI 3×3 were significantly better than those for CAIPI 3 × 3 and GRAPPA 3 × 3. Image noise was evident at the center for additional MPRAGE CAIPI 3 × 3 and GRAPPA 3 × 3. The correlation of segmentation results between GRAPPA 2 × 1 and Wave-CAIPI 3 × 3 was higher than 0.85 in all VOIs except globus pallidus. Subfield analysis of hippocampus also showed a high correlation between GRAPPA 2 × 1 and Wave-CAIPI 3 × 3.

Conclusion: MPRAGE Wave-CAIPI 3 × 3 shows relatively better contrast, despite of its short scan time of 1 min 42 s. The volumes derived from automated segmentation of MPRAGE Wave-CAIPI are considered to be reliable measures.

Keywords: *voxel-based morphometry, magnetization-prepared rapid gradient-echo, wave-controlled aliasing in parallel imaging, generalized autocalibrating partially parallel acquisition, subfield analysis*

[1]Department of Diagnostic Imaging and Nuclear Medicine, Graduate School of Medicine, Kyoto University, Kyoto, Kyoto, JAPAN

[2]Siemens Shenzhen Magnetic Resonance Ltd., Shenzhen, China

[3]Department of Neurology, Graduate School of Medicine, Kyoto University, Kyoto, Kyoto, JAPAN

[4]Human Brain Research Center, Graduate School of Medicine, Kyoto University, Kyoto, Kyoto, JAPAN

*Corresponding author: Department of Diagnostic Imaging and Nuclear Medicine, Graduate School of Medicine, Kyoto University, 54, Shogoin Kawaharacho, Sakyo-ku, Kyoto, Kyoto 606-8507, Japan. Phone: +81-75-751-3760, Fax: +81-75-771-9709, E-mail: yfushimi@kuhp.kyoto-u.ac.jp

Note: We presented a preliminary analysis of our data at ISMRM 2020. The data comprised a part of this manuscript.

Introduction

Voxel-based morphometry (VBM) is a robust technique to statistically analyze the local brain volume using MRI images.[1,2] VBM enables analysis of objective voxel estimation and provides us a clinically reliable tool to detect subtle anatomical changes in normal aging and neurodegenerative diseases.[3,4] VBM is usually calculated from high resolution 3D T1-weighted images (T1WI) after segmentation, and the neuroanatomical boundary is determined by the subtle differences in the image signal intensity and tissue contrast.[5,6]

Hippocampal volumetry has gained attention in the field of VBM,[7] and subfield estimation of hippocampus is used for evaluation and early diagnosis of dementia and temporal lobe epilepsy.[8,9] The reliability and validity issues have been investigated in comparison with manual hippocampal segmentation for younger and older brains.[10,11] Semi-automated hippocampal segmentation has been performed for cognitive impairment by using an age appropriate template;[12] however, automated hippocampal segmentation achieved hippocampal volume change measurement with the comparable reproducibility of expert manual outlining,[13] especially for the large MRI datasets including longitudinal studies for hippocampal atrophy.[14,15] High SNR is necessary for reliable results; however, 3D T1WI for VBM requires a relatively long scan time.[16]

Parallel imaging, such as generalized autocalibrating partially parallel acquisition (GRAPPA) and sensitivity encoding (SENSE), has been introduced to reduce scan time preserving SNR, and various scan time reduction techniques have been studied.[17,18] By taking advantage of coil sensitivity encoding from multi-channel receiver coils, reduction in phase-encoding steps has been available with the parallel imaging technique, such as SENSE and GRAPPA. Controlled aliasing in parallel imaging results in higher acceleration (CAIPIRINHA) has enabled image reconstruction with further acceleration.[19] Wave-controlled aliasing in parallel imaging (CAIPI) acquisition enables highly accelerated volumetric imaging with fewer artifacts and low SNR penalties by playing sinusoidal gradients during the readout of each phase encoding line.[16,20–25]

More acceleration has been expected with the introduction of Wave-CAIPI, but image quality has not been evaluated well in the clinical practice. Previous studies performed the image quality analysis by comparing optimized 6-min Wave-CAIPI examination protocols, including magnetization-prepared rapid gradient-echo (MPRAGE), 3D-T2, 3D-fluid-attenuated inversion recovery (FLAIR), and susceptibility weighted imaging (SWI) with the roughly 3× slower GRAPPA accelerated protocol.[26] Recent studies have shown the feasibility of application of applying Wave-CAIPI for quantitative susceptibility mapping[27] and SWI.[28,29] Visual examination of various parallel imaging algorithms, including Wave-CAIPI, has not been reported. In addition, a VBM study of MPRAGE Wave-CAIPI was investigated recently,[30] but subfield analysis of the hippocampus of MPRAGE Wave-CAIPI has not been performed thoroughly. In addition, no comparison between MPRAGE Wave-CAIPI and other parallel imaging methods, such as CAIPI and GRAPPA, has been reported.

We hypothesized that MPRAGE with 9-fold acceleration by using Wave-CAIPI (Wave-CAIPI 3 × 3) could be used reliably in clinical scanners. The purpose of this study was to perform the visual examination of MPRAGE Wave-CAIPI 3 × 3 and other parallel imaging methods, CAIPI 3 × 3, GRAPPA 2 × 1, and GRAPPA 3 × 3, to evaluate segmentation results of MPRAGE Wave-CAIPI 3 × 3 in VBM analysis.

Materials and Methods

Subjects

This study was approved by the institutional review board, and written informed consent was obtained from each subject. Twenty-seven healthy volunteers and 44 patients with neurological disorders were enrolled in this prospective study. Eleven patients were excluded due to severe head motion, cerebral infarction, and hemorrhage, and one healthy volunteer was excluded due to an incidental finding of ventriculomegaly. A total number of 26 healthy volunteers (16 men, 10 women, 25.9 years [23–36 years]) and 33 patients (19 men, 14 women, 65.3 years [23–88 years]) were included in this study (Fig. 1). The demographics of the included patients (n = 33) are as follows: white matter lesions, 17 (Fazekas grading: periventricular white matter, grade 3, 6; grade 2, 4; and grade 1, 7 and deep white matter, grade 3, 8; grade 2, 6; and grade 1, 3); dementia, 5; epilepsy, 4; motor neuron disease, 1; and miscellaneous (headache, 2; facial spasm, 1; loss of consciousness, 1; and benign fourth ventricle tumor, 1; and benign cerebellar tumor, 1). There were no trauma patients. All subjects were scanned with two MPRAGEs (GRAPPA 2 × 1 and Wave-CAIPI 3 × 3). Healthy volunteers underwent additional two MPRAGEs (CAIPI 3 × 3 and GRAPPA 3 × 3) for visual evaluation of image quality.

MR imaging

All the subjects underwent MR imaging at 3T MR scanners (MAGNETOM Prisma; Siemens Healthineers, Erlangen, Germany) with a 64-channel head/neck coil.

All MPRAGE scans used the following parameters in common: TR of 2300 ms, TE of 4.67 ms, flip angle of 9, and bandwidth of 130 Hz/pixel. Spatial resolution was isotropic 0.9 mm, and acquired slices were 208. For acceleration, 24 reference lines were acquired in the phase-encoding direction for all MPRAGEs, and reference lines in slice direction (and scan time) were as follows: (i) MPRAGE GRAPPA 2 × 1 (GRAPPA 2 × 1), not accelerated in slice direction (5 m 21 s). (ii) MPRAGE with a prototype Wave-CAIPI 3×3 (Wave-CAIPI 3 × 3) 24 reference lines in
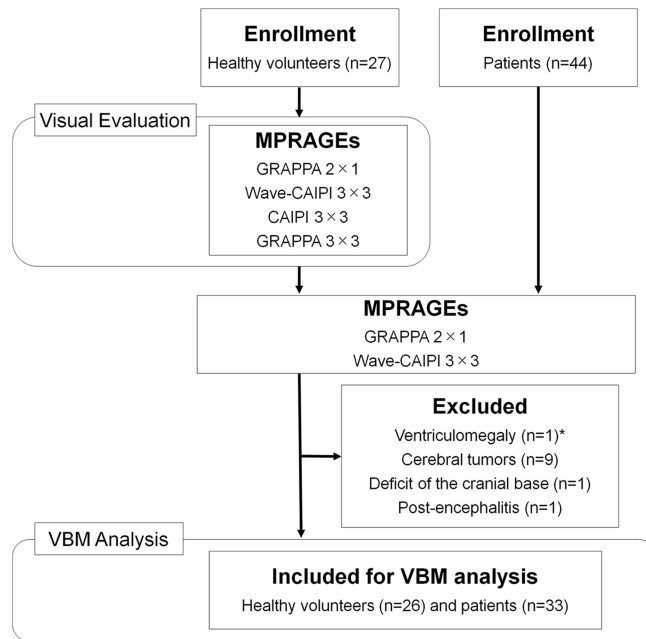
Fig. 1 The flow chart of the inclusion and exclusion of this study is shown. The asterisk (*) represents one subject that was excluded for the incidental abnormal finding listed in excluded reasons. The demographics of patients (n = 33) are as follows: chronic infarction or chronic ischemic white matter changes, 17; dementia, 5; epilepsy, 4; motor neuron disease, 1; and miscellaneous (headache, 2; facial spasm, 1; loss of consciousness, 1; benign fourth ventricle tumor, 1; and benign cerebellar tumor, 1). CAIPI, controlled aliasing in parallel imaging; GRAPPA, generalized autocalibrating partially parallel acquisition; MPRAGE, magnetization-prepared rapid gradient-echo; VBM, voxel-based morphometry.

slice direction with CAIPI shift factor of 1 (1 min 42 s). (iii) MPRAGE with CAIPIRINHA 3 × 3 (CAIPI 3 × 3); 24 reference lines with a CAIPI shift factor, 1 (1 min 42 s). (iv) MPRAGE GRAPPA 3 × 3 (GRAPPA 3 × 3); 24 reference lines (1 min 42 s) (Supplemental Table 1).

Evaluation of image quality
Three board certified radiologists (T.H., S.N., and Y.F.), with 11, 14, and 22 years of neuroradiology experience, respectively, performed the visual evaluation for the image quality of GRAPPA 2 × 1, Wave-CAIPI 3 × 3, CAIPI 3 × 3, and GRAPPA 3 × 3. All images were evaluated independently in a randomized and blinded fashion.[26]

We focused on image noise and the visualization of the corticomedullary junction of the cerebrum. The raters independently checked all MR images of GRAPPA 2 × 1, Wave-CAIPI 3 × 3, CAIPI 3 × 3, and GRAPPA 3 × 3 from each subject and scored image quality on a 5-point scale: 1, severe noise and hard to detect the corticomedullary junction; 2, overall low image quality and unclear visualization of the corticomedullary junction; 3, low image quality in the center and partly unclear visualization of the corticomedullary junction; 4, less image noise in the center and clear visualization of the corticomedullary junction; and 5, no image noise and excellent visualization of the corticomedullary junction. Representative images corresponding to each grade are shown in Supplemental Fig. 1.

Disagreements on evaluation were resolved by discussion among the raters.

VBM analysis including subfield analysis
We also performed VBM analysis by using the recon-all function of FreeSurfer (v6.0.1) (http://surfer.nmr.mgh.harvard.edu/) for MPRAGE images with clear visualization of corticomedullary junction (scores of 4 and 5).[31] The parcellation status was visually checked and voxel sizes of VOIs were compared. We also performed subfield analysis for the hippocampus of FreeSurfer,[32] and the results were compared. We also performed additional volumetric calculation by using segmentation function of CAT12 with SPM12.[33]

SNR calculation
An aqueous copper sulfate phantom with a cylindrical, plastic bottle phantom (1.9 L, 5g NaCl, 3.75g $NiSO_4 × 6H_2O$ per 1000 g water) was scanned with four MPRAGEs of GRAPPA 2 × 1, Wave-CAIPI 3 × 3, CAIPI 3 × 3, and GRAPPA 3 × 3. Each MPRAGE was scanned 10 times, and the SNR of each MPRAGE was calculated as the average divided by the standard deviation.

Statistical analysis
The interobserver agreement for the qualitative scores was assessed by calculating the intraclass correlation coefficient (ICC). ICC and its 95% confidence intervals (CIs) were calculated by using a two-way random absolute single measures model ICC (2,1).

Medians and mean ranks were calculated and compared by using Friedman test. In the case of significant
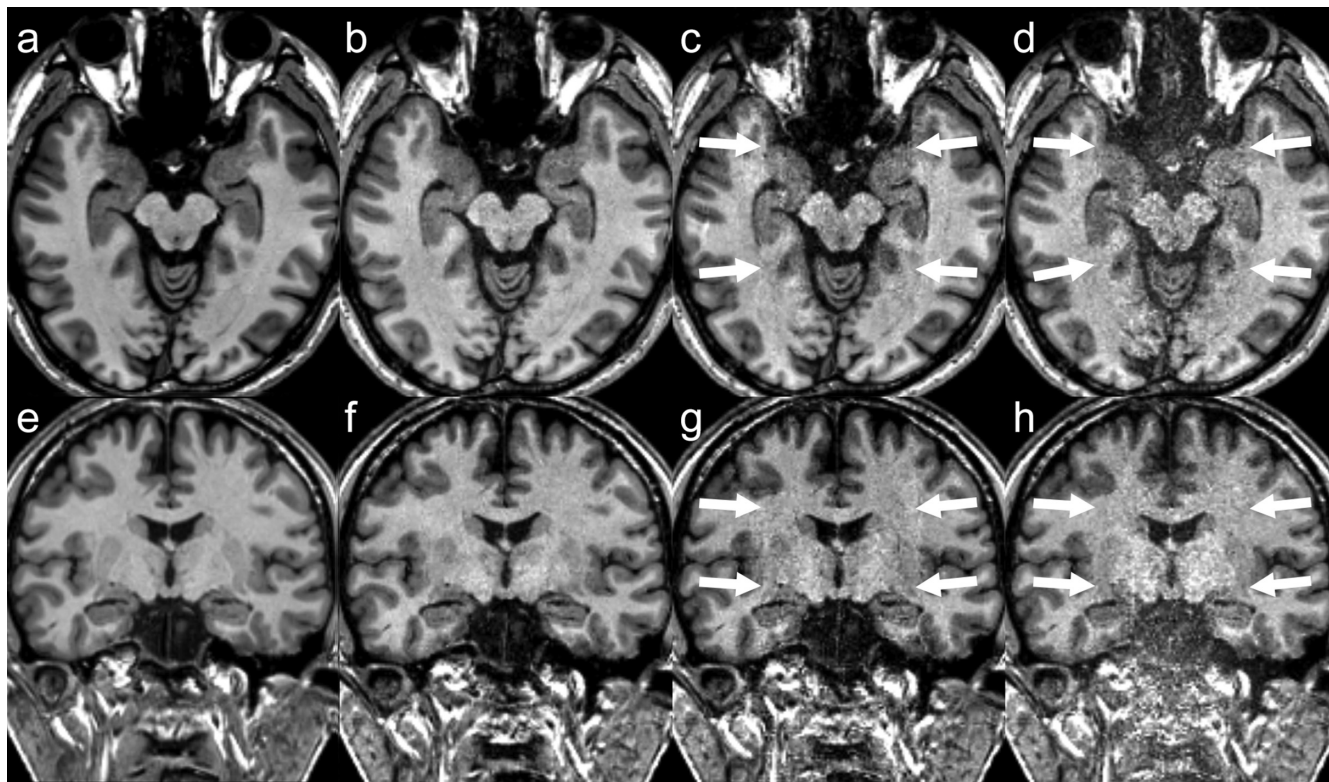
Fig. 2 A 26-year-old man, a healthy volunteer. MPRAGE images of GRAPPA 2 × 1 (**a** and **e**), Wave-CAIPI 3 × 3 (**b** and **f**), CAIPI 3 × 3 (**c** and **g**), and GRAPPA 3 × 3 (**d** and **h**) are shown. Note that image degradation at the center part is evident in CAIPI 3 × 3 and GRAPPA 3 × 3 (arrows). CAIPI, controlled aliasing in parallel imaging; GRAPPA, generalized autocalibrating partially parallel acquisition; MPRAGE, magnetization-prepared rapid gradient-echo.

results, post-hoc analysis was performed by using Wilcoxon signed-rank test. Reproducibility was analyzed by ICC.

Correlation of segmentation results (i.e. volume of each structure) between the two MPRAGEs was analyzed by Pearson's correlation coefficient if the data were normally distributed. If the normality of data was rejected, Spearman's signed-rank test was used. Bland-Altman analysis was also performed for the segmentation results.

Statistical analysis was performed by using Medcalc version 18 (MedCalc Software, Ostend, Belgium) and JMP Pro version 14.0 (SAS Institute, Cary, NC, USA).

Results

Representative MPRAGE images of GRAPPA 2 × 1, Wave-CAIPI 3 × 3, CAIPI 3 × 3, and GRAPPA 3 × 3 are shown for a healthy volunteer (Fig. 2). Image noise was evident at the center in CAIPI 3 × 3 and GRAPPA 3 × 3 in all healthy volunteers.

Fusion images of MPRAGE with parcellation results of recon-all function and fusion images of those with parcellation results of subfield analysis for a healthy volunteer and a patient are shown in Figs. 3 and 4, respectively.

Evaluation of image quality
The image quality analysis results for MPRAGE images of GRAPPA 2 × 1, Wave-CAIPI 3 × 3, CAIPI 3 × 3, and GRAPPA 3 × 3 are shown in Fig. 5. The overall scores (median [mean $\pm$ SD]) for the MPRAGEs of GRAPPA 2 × 1, Wave-CAIPI 3 × 3, CAIPI 3 × 3, and GRAPPA 3 × 3 (5 [5.00 $\pm$ 0.00], 4 [4.00 $\pm$ 0.00], 3 [2.65 $\pm$ 0.49], and 2 [2.00 $\pm$ 0.00], respectively) showed good agreement. The scores for GRAPPA 2 × 1 were significantly better than those for Wave-CAIPI 3 × 3, CAIPI 3 × 3, and GRAPPA 3 × 3 ($P < 0.001$) and the scores for Wave-CAIPI 3 × 3 were the best among Wave-CAIPI 3 × 3, CAIPI 3 × 3, and GRAPPA 3 × 3 ($P < 0.001$). ICC among the three raters was 0.97 (CI 0.96–0.98). The values inside the parenthesis represent 95% CI.

Friedman test revealed that the image quality of GRAPPA 2 × 1 (mean rank: 4.00) was significantly better than that of Wave-CAIPI 3 × 3 (mean rank: 3.00), CAIPI 3 × 3 (mean rank: 1.83), and GRAPPA 3 × 3 (mean rank: 1.17). Post-hoc analysis showed that the image quality of GRAPPA 2 × 1, Wave-CAIPI 3 × 3, GRAPPA 2 × 1, and CAIPI 3 × 3 significantly varied.

VBM analysis
Based on the results of the visual evaluation, VBM analyses, including subfield analysis, were performed only for
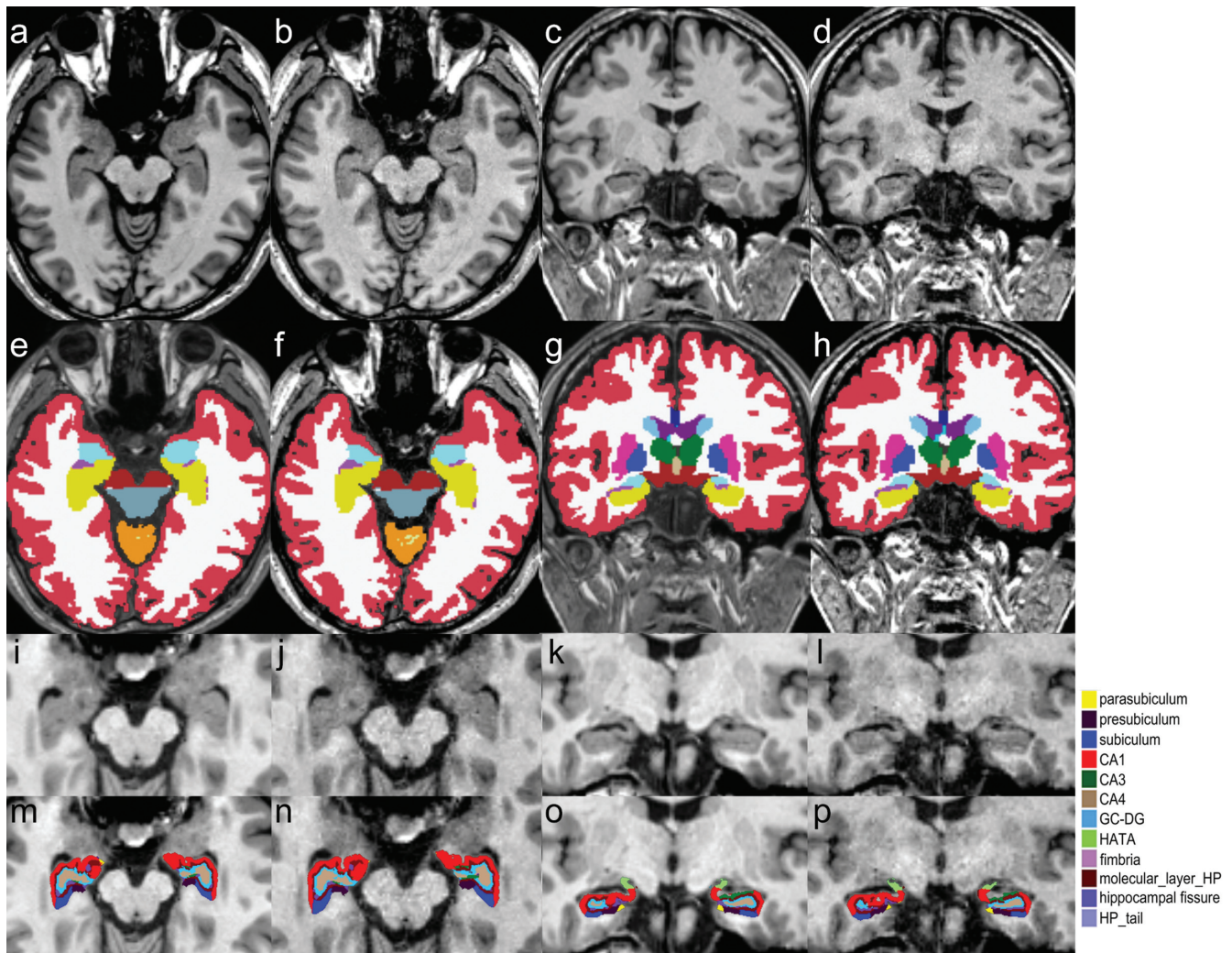
Fig. 3 A 26-year-old man, a healthy volunteer. MPRAGE images of GRAPPA 2 × 1 (**a** and **c**) and Wave-CAIPI 3 × 3 (**b** and **d**) are shown. Fusion images of MPRAGE with parcellation results are also shown (GRAPPA 2 × 1, **e** and **g**; Wave-CAIPI 3 × 3, **f** and **h**). Enlarged images of hippocampi on MPRAGE images of GRAPPA 2 × 1 (**i** and **k**) and Wave-CAIPI 3 × 3 (**j** and **l**), and fusion images of subfield analysis of GRAPPA 2 × 1 (**m** and **o**) and Wave-CAIPI 3 × 3 (**n** and **p**) are shown. Almost identical parcellation results are shown in all MPRAGE images. CAIPI, controlled aliasing in parallel imaging; GC-DG, granule cell layer of the dentate gyrus; GRAPPA, generalized autocalibrating partially parallel acquisition; HATA, hippocampal-amygdaloid transition region; MPRAGE, magnetization-prepared rapid gradient-echo.

GRAPPA 2 × 1 and Wave-CAIPI 3 × 3. No segmentation errors in the recon-all function in FreeSurfer were found for either of the MPRAGEs with GRAPPA 2 × 1 and Wave-CAIPI 3 × 3 in our cohort. We measured the volumes of each VOI created from recon-all function and subfield analysis between GRAPPA 2 × 1 and Wave-CAIPI 3 × 3 (Tables 1–4, Figs. 6 and 7, Supplemental Figures 2–5).

The correlation between GRAPPA 2 × 1 and Wave-CAIPI 3 × 3 was higher than 0.85 in all VOIs, except for globus pallidus (Table 1). The correlation between GRAPPA 2 × 1 and Wave-CAIPI 3 × 3 was comparable or better in patients than that in healthy volunteers, except for the caudate, globus pallidus, and hippocampus (Table 3).

The results for the deep gray matter, hippocampus, and amygdala are shown in Fig. 6. The correlation coefficient of most VOIs were higher than 0.9. The correlations between GRAPPA 2 × 1 and Wave-CAIPI 3 × 3 in cerebral cortex and cerebral white matter were very high (0.98 and 0.99, respectively) (Fig. 6).

Additional segmentation results derived from SPM12 are shown in Supplemental Table 2. The correlations between GRAPPA 2 × 1 and Wave-CAIPI 3 × 3 were very good in the segmentation results using LBPA40 atlas.[34]

Bland-Altman analysis was performed between the measurements of GRAPPA 2 × 1 and Wave-CAIPI 3 × 3, and most of the data were distributed between ±1.96 SD (Supplemental Figure 6).
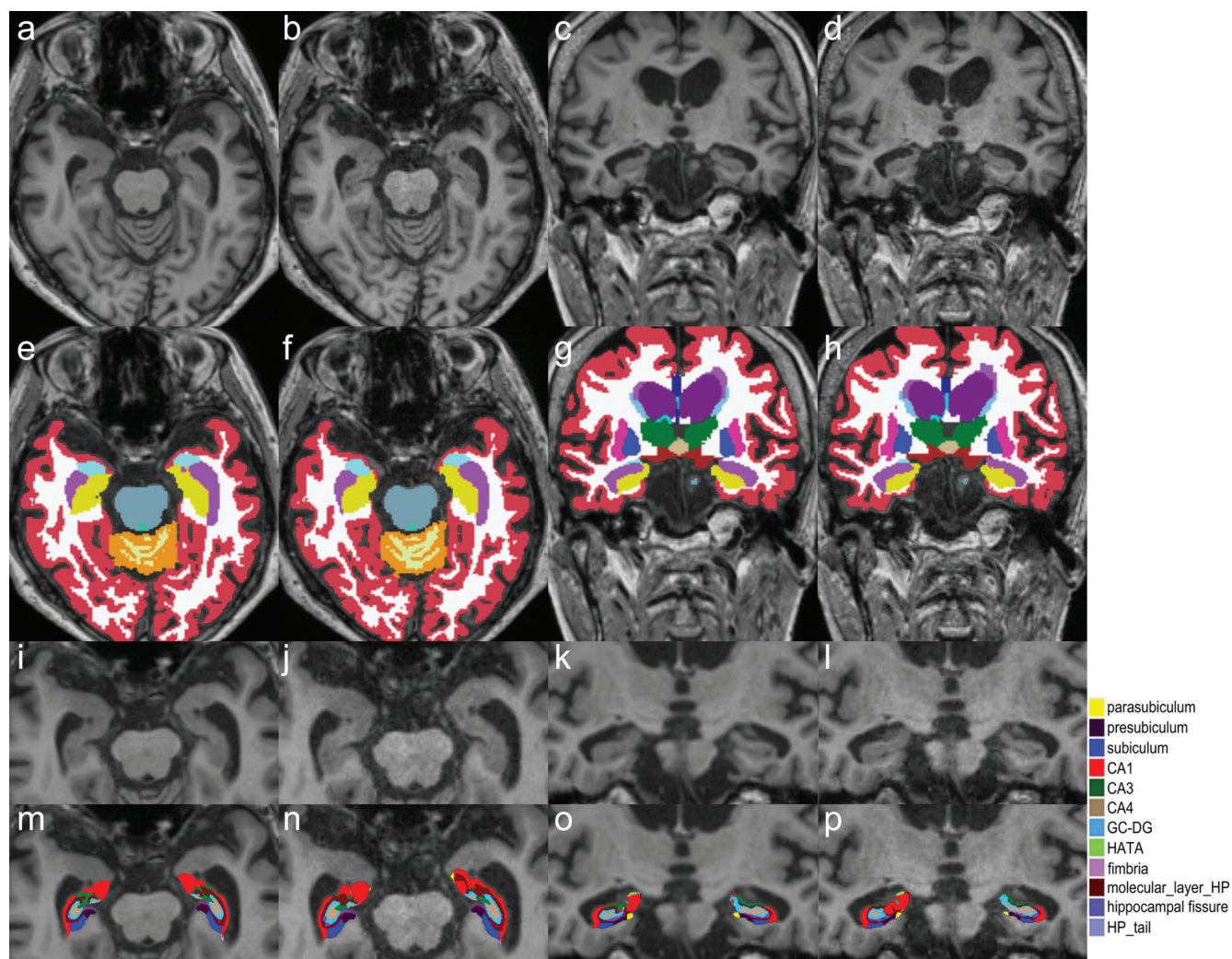
Fig. 4 An 81 year-old woman with dementia. MPRAGE images of GRAPPA 2 × 1 (**a** and **c**) and Wave-CAIPI 3 × 3 (**b** and **d**) are shown. The atrophy of bilateral left temporal lobe including hippocampi is evident. Fusion images of MPRAGE with parcellation results are also shown (GRAPPA 2 × 1, **e** and **g**; Wave-CAIPI 3 × 3, **f** and **h**). Enlarged images of hippocampi on MPRAGE images of GRAPPA 2 × 1 (**i** and **k**) and Wave-CAIPI 3 × 3 (**j** and **l**), and fusion images of subfield analysis of GRAPPA 2 × 1 (**m** and **o**) and Wave-CAIPI 3 × 3 (**n** and **p**) are shown. Almost identical parcellation results are shown in all MPRAGE images even in patients with dementia. CAIPI, controlled aliasing in parallel imaging; GC-DG, granule cell layer of the dentate gyrus; GRAPPA, generalized autocalibrating partially parallel acquisition; HATA, hippocampal-amygdaloid transition region; MPRAGE, magnetization-prepared rapid gradient-echo.

Subfield analysis of hippocampus

The volumes of CA1 measured in GRAPPA 2 × 1 and Wave-CAIPI 3 × 3 were 632.77 ± 95.44 mm^3 and 630.40 ± 92.39 mm^3 on the right and were 663.74 ± 95.65 mm^3 and 659.32 ± 96.88 mm^3 on the left. The correlations of CA1 between GRAPPA 2 × 1 and Wave-CAIPI 3 × 3 were 0.93 ($P < 0.001$) on the right and 0.94 ($P < 0.001$) on the left. The correlations of subiculum were 0.94 ($P < 0.001$) on the right and were 0.95 ($P < 0.001$) on the left. The details of subfield analysis are shown in Table 2, 4, and Fig. 7.

As in the results of the statistical output from the subcortical segmentation or aseg_stats, the correlation between GRAPPA 2 × 1 and Wave-CAIPI 3 × 3 in patients were comparable or better than in healthy volunteers, except for the parasubiculum (Table 4).

SNR map

SNR maps of MPRAGE images of GRAPPA 2 × 1, Wave-CAIPI 3 × 3, CAIPI 3 × 3, and GRAPPA 3 × 3 are shown in Fig. 8. GRAPPA 2 × 1 showed the highest SNR among the four MPRAGEs. SNR map of Wave-CAIPI 3 × 3 showed higher SNR than that of CAIPI 3×3 and GRAPPA 3 × 3.
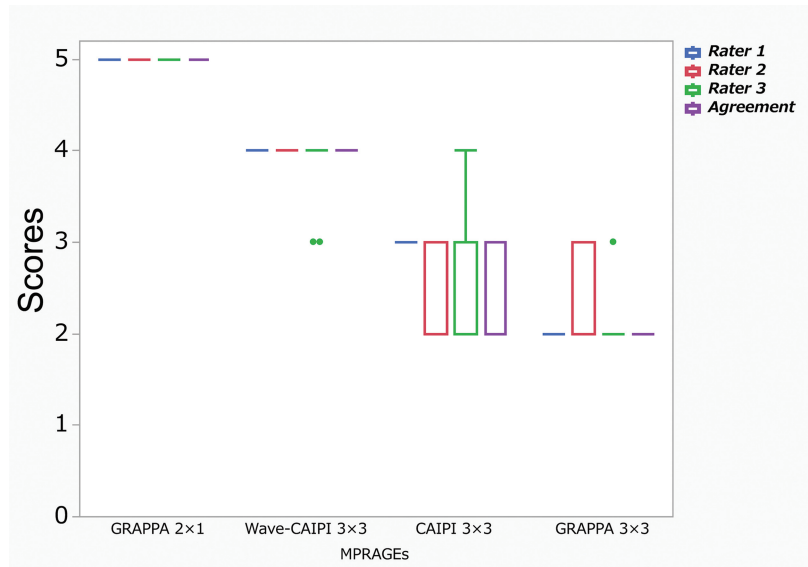
Fig. 5 The box and whisker plot showed image quality analysis results for MPRAGE images of GRAPPA 2 × 1, Wave-CAIPI 3 × 3, CAIPI 3 × 3, and GRAPPA 3 × 3. The image noise and signal uniformity were evaluated in the center part of the images, and delineation of cortico-medullary junction at the level of putamen. Disagreements on evaluation were resolved by discussion among raters and the overall final scores (median [mean $\pm$ SD]) for both MPRAGEs of GRAPPA 2 × 1, Wave-CAIPI 3 × 3, CAIPI 3 × 3, and GRAPPA 3 × 3 were 5 (5.00 $\pm$ 0.00), 4 (4.00 $\pm$ 0.00), 3 (2.65 $\pm$ 0.49), and 2 (2.00 $\pm$ 0.00), respectively. CAIPI, controlled aliasing in parallel imaging; GRAPPA, generalized autocalibrating partially parallel acquisition; MPRAGE, magnetization-prepared rapid gradient-echo.

Table 1 The results of recon-all function of all subjects.

Volume of interest		All subjects (n = 59)		
		GRAPPA 2 × 1	Wave-CAIPI 3 × 3	Correlation coefficient (*P* value)
Thalamus-Proper	Lt.	7238.69 $\pm$ 1100.91	7241.36 $\pm$ 1081.95	0.93 (*P* < 0.001)
	Rt.	6970.04 $\pm$ 953.76	7066.00 $\pm$ 1032.82	0.92 (*P* < 0.001)
Caudate	Lt.	3421.03 $\pm$ 563.48	3449.52 $\pm$ 606.19	0.96 (*P* < 0.001)
	Rt.	3552.22 $\pm$ 512.19	3695.31 $\pm$ 595.89	0.91 (*P* < 0.001)
Putamen	Lt.	4619.13 $\pm$ 822.17	4785.88 $\pm$ 811.46	0.94* (*P* < 0.001)
	Rt.	4792.39 $\pm$ 812.36	4834.17 $\pm$ 787.68	0.92 (*P* < 0.001)
Pallidum	Lt.	2071.15 $\pm$ 292.43	2032.36 $\pm$ 297.46	0.82* (*P* < 0.001)
	Rt.	1925.90 $\pm$ 185.54	1892.75 $\pm$ 243.27	0.68 (*P* < 0.001)
Hippocampus	Lt.	3956.73 $\pm$ 555.14	3935.99 $\pm$ 573.10	0.93* (*P* < 0.001)
	Rt.	4108.26 $\pm$ 565.02	4120.25 $\pm$ 561.98	0.94 (*P* < 0.001)
Amygdala	Lt.	1565.16 $\pm$ 289.11	1567.09 $\pm$ 291.98	0.85* (*P* < 0.001)
	Rt.	1679.90 $\pm$ 267.88	1623.57 $\pm$ 277.55	0.90 (*P* < 0.001)
Cortex Vol	Lt.	233165.08 $\pm$ 31173.56	234259.90 $\pm$ 32641.60	0.99* (*P* < 0.001)
	Rt.	233633.10 $\pm$ 30299.30	235557.49 $\pm$ 31688.99	0.99 (*P* < 0.001)
Cerebral White Matter Vol	Lt.	224294.07 $\pm$ 28873.58	217285.31 $\pm$ 32079.32	0.99* (*P* < 0.001)
	Rt.	224007.75 $\pm$ 28939.66	217346.87 $\pm$ 31245.14	0.99* (*P* < 0.001)

The volume data were shown in mean $\pm$ SD (mm³). Correlation coefficient of segmentation results between GRAPPA 2×1 and Wave-CAIPI 3×3 was shown with R if the data show normal distribution. If the normality of data is rejected, ρ was shown (*). CAIPI, controlled aliasing in parallel imaging; GRAPPA, generalized autocalibrating partially parallel acquisition; Lt., left; Rt., right.

Table 2 The results of subfield analysis of all subjects

Volume of interest		All subjects (n=59)		
		GRAPPA 2×1	Wave-CAIPI 3×3	Correlation coefficient (*P* value)
Hippocampal_tail	Lt.	508.70 ± 89.18	517.17 ± 97.36	0.92 (*P* < 0.001)
	Rt.	537.80 ± 77.57	549.49 ± 93.83	0.92 (*P* < 0.001)
Subiculum	Lt.	433.18 ± 58.82	431.09 ± 61.75	0.93* (*P* < 0.001)
	Rt.	434.74 ± 67.03	438.90 ± 69.06	0.91* (*P* < 0.001)
CA1	Lt.	632.77 ± 95.44	630.40 ± 92.39	0.92* (*P* < 0.001)
	Rt.	663.74 ± 95.65	659.32 ± 96.88	0.94* (*P* < 0.001)
Hippocampal-fissure	Lt.	157.10 ± 30.40	161.37 ± 31.65	0.63* (*P* < 0.001)
	Rt.	168.09 ± 38.90	174.42 ± 29.17	0.74* (*P* < 0.001)
Presubiculum	Lt.	291.59 ± 44.51	297.89 ± 46.21	0.80* (*P* < 0.001)
	Rt.	282.90 ± 54.14	295.63 ± 57.58	0.85* (*P* < 0.001)
Parasubiculum	Lt.	58.31 ± 12.27	61.30 ± 13.08	0.76 (*P* < 0.001)
	Rt.	53.02 ± 13.28	55.55 ± 13.22	0.89* (*P* < 0.001)
Molecular_layer_HP	Lt.	561.51 ± 83.03	555.53 ± 82.16	0.94* (*P* < 0.001)
	Rt.	577.46 ± 85.51	571.71 ± 86.78	0.95* (*P* < 0.001)
GC-ML-DG	Lt.	298.10 ± 46.74	291.62 ± 47.11	0.90* (*P* < 0.001)
	Rt.	307.24 ± 47.88	297.08 ± 46.60	0.92 (*P* < 0.001)
CA3	Lt.	205.70 ± 34.01	197.57 ± 31.76	0.91 (*P* < 0.001)
	Rt.	220.28 ± 34.24	209.01 ± 33.87	0.85* (*P* < 0.001)
CA4	Lt.	256.03 ± 37.42	249.41 ± 38.52	0.86* (*P* < 0.001)
	Rt.	263.72 ± 37.96	253.45 ± 37.37	0.90* (*P* < 0.001)
Fimbria	Lt.	82.46 ± 26.11	86.71 ± 24.77	0.78* (*P* < 0.001)
	Rt.	77.54 ± 30.38	81.84 ± 30.76	0.93* (*P* < 0.001)
HATA	Lt.	58.45 ± 9.82	58.15 ± 9.48	0.80 (*P* < 0.001)
	Rt.	60.74 ± 10.59	60.54 ± 10.25	0.74* (*P* < 0.001)
Whole_hippocampus	Lt.	3386.81 ± 473.01	3376.84 ± 480.51	0.94* (*P* < 0.001)
	Rt.	3479.19 ± 487.35	3472.52 ± 506.00	0.95* (*P* < 0001)

The volume data were shown as mean ± SD (mm³). Correlation coefficient of segmentation results between GRAPPA 2×1 and Wave-CAIPI 3×3 was shown with R if the data show normal distribution. If the normality of data is rejected, ρ was shown (*). CAIPI, controlled aliasing in parallel imaging; GC-ML-DG, granule cell and molecular layer of the dentate gyrus; GRAPPA, generalized autocalibrating partially parallel acquisition; HATA, hippocampal-amygdaloid transition region; HP, hippocampus; Lt., left; Rt., right.

Discussion

In this study, visual examination of four different MPRAGEs, including Wave-CAIPI 3 × 3, was performed to evaluate the segmentation results of MPRAGE Wave-CAIPI 3 × 3. Fewer image degradations at the center of images were observed in Wave-CAIPI 3 × 3 than in the CAIPI 3 × 3 or GRAPPA 3 × 3; thus, Wave-CAIPI 3 × 3 scores were maintained with a reduced scan time. Scores and ICCs were slightly low partly because the patients with diseases included ischemic changes, dilated perivascular spaces, and neurodegenerative diseases. The boundary of deep gray matter and the surrounding white matter tended to be obscure in patients, which may have affected the mild discrepancy between raters.

VBM analysis and subfield analysis were also performed for MPRAGE images with clear visualization of corticomedullary junction (GRAPPA 2 × 1 and Wave-CAIPI 3 × 3). No segmentation error was found in MPRAGE Wave-CAIPI 3 × 3. A short scan time of Wave-CAIPI can reduce motion artifacts, and high SNR derived from the 64-channel phased array coil may

Table 3 The results of recon-all function of healthy volunteers and patients

Volume of interest		Healthy volunteers (n=26)			Patients (n=33)		
		GRAPPA 2×1	Wave-CAIPI 3×3	Correlation coefficient (*P* value)	GRAPPA 2×1	Wave-CAIPI 3×3	Correlation coefficient (*P* value)
Thalamus-Proper	Lt.	7985.06 ± 651.64	8022.71 ± 615.81	0.84 (*P* < 0.001)	6650.64 ± 1023.55	6625.76 ± 966.52	0.91 (*P* < 0.001)
	Rt.	7633.82 ± 686.12	7758.75 ± 718.54	0.81 (*P* < 0.001)	6447.06 ± 796.75	6520.20 ± 907.95	0.91 (*P* < 0.001)
Caudate	Lt.	3634.19 ± 435.96	3674.03 ± 475.70	0.90* (*P* < 0.001)	3253.09 ± 594.91	3272.63 ± 638.51	0.95 (*P* < 0.001)
	Rt.	3674.94 ± 445.76	3841.53 ± 495.44	0.94* (*P* < 0.001)	3455.53 ± 539.68	3580.10 ± 641.36	0.89 (*P* < 0.001)
Putamen	Lt.	4959.68 ± 416.66	5155.99 ± 345.97	0.86 (*P* < 0.001)	4350.81 ± 953.1	4494.29 ± 943.4	0.97* (*P* < 0.001)
	Rt.	5154.03 ± 434.50	5214.38 ± 392.25	0.78 (*P* < 0.001)	4507.46 ± 920.28	4534.62 ± 885.68	0.92 (*P* < 0.001)
Pallidum	Lt.	2133.28 ± 202.24	2191.20 ± 186.91	0.81 (*P* < 0.001)	2022.20 ± 339.46	1907.21 ± 308.44	0.81* (*P* < 0.001)
	Rt.	1956.48 ± 151.35	1958.41 ± 176.39	0.65 (*P* < 0.001)	1901.81 ± 205.38	1841.02 ± 274.27	0.68 (*P* < 0.001)
Hippocampus	Lt.	4176.32 ± 291.96	4209.10 ± 319.30	0.89 (*P* < 0.001)	3783.73 ± 644.91	3720.82 ± 633.89	0.94 (*P* < 0.001)
	Rt.	4320.73 ± 319.69	4378.00 ± 412.60	0.86* (*P* < 0.001)	3940.86 ± 653.19	3917.18 ± 580.47	0.68 (*P* < 0.001)
Amygdala	Lt.	1750.75 ± 200.51	1740.17 ± 190.37	0.63* (*P* < 0.001)	1418.95 ± 263.15	1430.72 ± 285.77	0.89 (*P* < 0.001)
	Rt.	1835.17 ± 144.31	1772.51 ± 185.41	0.76 (*P* < 0.001)	1557.58 ± 279.17	1506.23 ± 281.76	0.91 (*P* < 0.001)
CortexVol	Lt.	256478.58 ± 17431.98	258042.34 ± 18633.75	0.99* (*P* < 0.001)	214796.86 ± 27063.07	215522.22 ± 28890.22	0.98* (*P* < 0.001)
	Rt.	255708.01 ± 18346.84	258579.19 ± 18590.07	0.99 (*P* < 0.001)	216240.75 ± 26262.60	217419.19 ± 27866.05	0.98 (*P* < 0.001)
Cerebral White Matter Vol	Lt.	237948.53 ± 18359.06	232727.82 ± 18548.47	0.99 (*P* < 0.001)	213536.01 ± 31021.53	205118.49 ± 35112.55	0.99* (*P* < 0.001)
	Rt.	237173.11 ± 18817.02	231578.45 ± 18610.78	0.98 (*P* < 0.001)	213635.05 ± 31212.65	206134.11 ± 34456.36	0.99 (*P* < 0.001)

The volume data were shown as mean ± SD (mm³). Correlation coefficient of segmentation results between GRAPPA 2×1 and Wave-CAIPI 3×3 was shown with R if the data show normal distribution. If the normality of data is rejected, ρ was shown (*). CAIPI, controlled aliasing in parallel imaging; GRAPPA, generalized autocalibrating partially parallel acquisition; Lt., left; Rt., right.
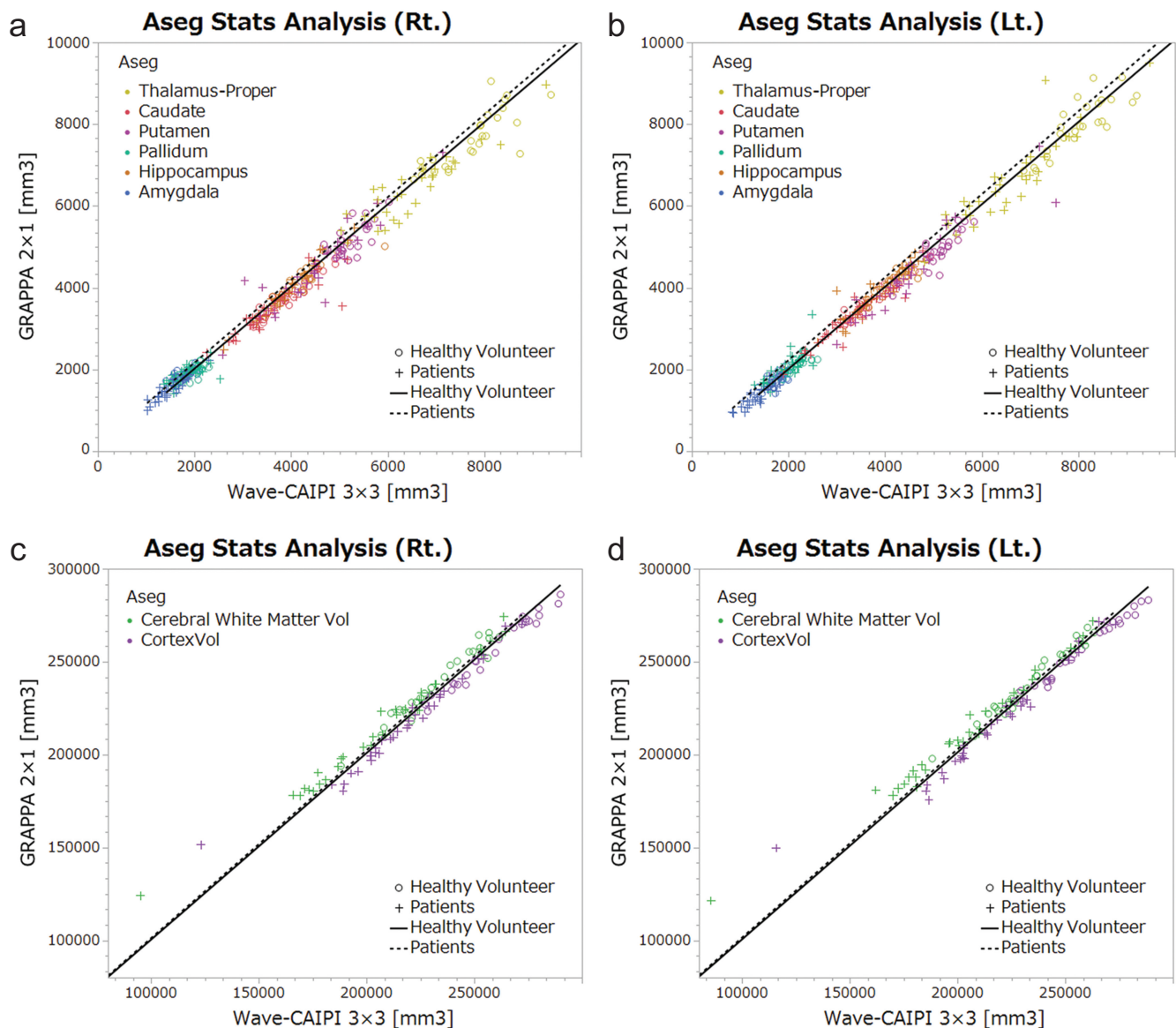
Fig. 6 The volumetric results of deep gray matters, hippocampus and amygdala (right, **a** and left, **b**) and those of cerebral cortex and white matter (right, **c** and left, **d**) are shown. The correlation efficient of most VOIs were higher than 0.85 except globus pallidus. The correlation between GRAPPA 2 × 1 and Wave-CAIPI 3 × 3 in cerebral cortex and cerebral white matter was very high (0.98 and 0.99, respectively). CAIPI, controlled aliasing in parallel imaging; GRAPPA, generalized autocalibrating partially parallel acquisition; Lt., left; Rt., right. VOI, voxel of interest.

contribute to the relatively good image quality. The correlation between the cerebral cortex and cerebral white matter was very high (0.98–0.99). MPRAGE Wave-CAIPI 3 × 3 showed that the correlation of VOIs were > 0.85 in deep gray matters, except for globus pallidus or hippocampus. The correlations of globus pallidus and amygdala were relatively lower than that of other VOIs. This is probably because globus pallidus and amygdala are relatively small in volume. In addition, globus pallidus and amygdala show less image contrast on both MPRAGE GRAPPA 2 × 1 and Wave-CAIPI 3 × 3; therefore, parcellation of

these VOIs was derived from probabilistic image segmentation.

Hippocampal subfield analysis gains attention because synaptic and neuronal losses lead to structural alterations, and various associations were found between hippocampal subfields and neurological diseases. Early stage of Alzheimer's disease (AD) showed that neurofibrillary tangle accumulation and neuron loss are more prominent in the CA1 and subiculum.[35] On the contrary, volumetric study revealed that CA1 was least involved in the AD-associated atrophy,[36] and presubiculum and subiculum progressively

Table 4 The results of subfield analysis of healthy volunteers and patients

Volume of interest		Healthy volunteers (n=26)			Patients (n=33)		
		GRAPPA 2×1	Wave-CAIPI 3×3	Correlation coefficient (*P* value)	GRAPPA 2×1	Wave-CAIPI 3×3	Correlation coefficient (*P* value)
Hippocampal tail	Lt.	546.78 ± 63.66	565.94 ± 57.38	0.71* (*P* < 0.001)	478.69 ± 94.79	478.74 ± 104.90	0.94 (*P* < 0.001)
	Rt.	569.00 ± 52.93	589.29 ± 66.89	0.72 (*P* < 0.001)	513.50 ± 83.74	520.65 ± 99.36	0.97 (*P* < 0.001)
Subiculum	Lt.	450.00 ± 38.94	452.72 ± 41.97	0.87 (*P* < 0.001)	419.93 ± 67.76	414.05 ± 69.07	0.96* (*P* < 0.001)
	Rt.	457.92 ± 54.26	470.09 ± 61.66	0.85* (*P* < 0.001)	418.97 ± 70.07	417.19 ± 64.45	0.96 (*P* < 0.001)
CA1	Lt.	660.19 ± 59.93	658.06 ± 61.77	0.87 (*P* < 0.001)	611.17 ± 111.34	608.61 ± 105.73	0.95 (*P* < 0.001)
	Rt.	694.69 ± 68.43	683.87 ± 87.11	0.85* (*P* < 0.001)	639.54 ± 105.12	641.25 ± 98.57	0.98 (*P* < 0.001)
Hippocampal fissure	Lt.	145.82 ± 21.33	158.20 ± 24.92	0.51 (P=0.008)	165.98 ± 33.38	163.88 ± 35.88	0.77 (*P* < 0.001)
	Rt.	148.05 ± 25.00	167.74 ± 25.31	0.66 (*P* < 0.001)	181.77 ± 40.83	178.14 ± 30.71	0.84 (*P* < 0.001)
Presubiculum	Lt.	313.22 ± 34.66	323.68 ± 29.98	0.81 (*P* < 0.001)	274.54 ± 44.01	277.57 ± 46.61	0.80 (*P* < 0.001)
	Rt.	311.55 ± 46.66	325.32 ± 52.05	0.77* (*P* < 0.001)	265.52 ± 50.02	276.47 ± 51.39	0.91 (*P* < 0.001)
Parasubiculum	Lt.	63.82 ± 9.60	66.44 ± 8.22	0.86 (*P* < 0.001)	53.96 ± 12.40	57.25 ± 14.68	0.68 (*P* < 0.001)
	Rt.	58.97 ± 9.60	60.86 ± 8.24	0.85 (*P* < 0.001)	49.16 ± 13.96	51.74 ± 14.73	0.90 (*P* < 0.001)
Molecular_layer HP	Lt.	591.17 ± 48.93	591.17 ± 50.67	0.88 (*P* < 0.001)	538.15 ± 95.92	527.44 ± 90.86	0.97* (*P* < 0.001)
	Rt.	612.90 ± 55.34	610.66 ± 74.16	0.85* (*P* < 0.001)	551.77 ± 93.76	543.66 ± 83.21	0.98 (*P* < 0.001)
GC-ML-DG	Lt.	314.86 ± 24.86	314.96 ± 28.42	0.77 (*P* < 0.001)	284.90 ± 54.99	273.22 ± 50.63	0.97 (*P* < 0.001)
	Rt.	321.55 ± 27.39	314.85 ± 39.24	0.74* (*P* < 0.001)	296.62 ± 56.25	284.58 ± 46.90	0.98 (*P* < 0.001)
CA3	Lt.	212.77 ± 22.51	208.00 ± 22.44	0.80 (*P* < 0.001)	200.14 ± 39.99	189.36 ± 35.41	0.95 (*P* < 0.001)
	Rt.	225.65 ± 26.57	218.34 ± 34.50	0.78* (*P* < 0.001)	215.25 ± 38.17	201.13 ± 30.78	0.93 (*P* < 0.001)
CA4	Lt.	267.14 ± 21.40	267.59 ± 25.16	0.73 (*P* < 0.001)	247.28 ± 44.37	235.10 ± 41.10	0.96 (*P* < 0.001)
	Rt.	271.89 ± 23.40	265.65 ± 34.69	0.72* (*P* < 0.001)	257.35 ± 44.81	244.46 ± 36.17	0.96 (*P* < 0.001)
Fimbria	Lt.	98.71 ± 14.50	100.90 ± 20.11	0.49 (*P* = 0.011)	69.66 ± 26.10	75.53 ± 22.24	0.86 (*P* < 0.001)
	Rt.	94.95 ± 20.85	98.05 ± 23.14	0.88 (*P* < 0.001)	66.09 ± 30.21	71.48 ± 30.49	0.94 (*P* < 0.001)
HATA	Lt.	62.18 ± 6.46	62.11 ± 7.79	0.65 (*P* < 0.001)	55.52 ± 10.96	55.02 ± 9.53	0.82 (*P* < 0.001)
	Rt.	65.34 ± 6.76	64.61 ± 7.91	0.66 (*P* < 0.001)	57.61 ± 11.62	57.85 ± 10.74	0.81 (*P* < 0.001)
Whole hippocampus	Lt.	3580.85 ± 279.17	3611.58 ± 274.32	0.90 (*P* < 0.001)	3233.93 ± 534.40	3191.89 ± 525.26	0.98* (*P* < 0.001)
	Rt.	3684.39 ± 320.91	3701.59 ± 419.28	0.87* (*P* < 0.001)	3331.37 ± 530.46	3310.45 ± 494.04	0.98 (*P* < 0.001)

The volume data were shown as mean ± SD (mm^3). Correlation coefficient of segmentation results between GRAPPA 2×1 and Wave-CAIPI 3×3 was shown with R if the data show normal distribution. If the normality of data is rejected, ρ was shown (*). CAIPI, controlled aliasing in parallel imaging; GC-ML-DG, granule cell and molecular layer of the dentate gyrus; GRAPPA, generalized autocalibrating partially parallel acquisition; HATA, hippocampal-amygdaloid transition region; HP, hippocampus; Lt., left; Rt., right.
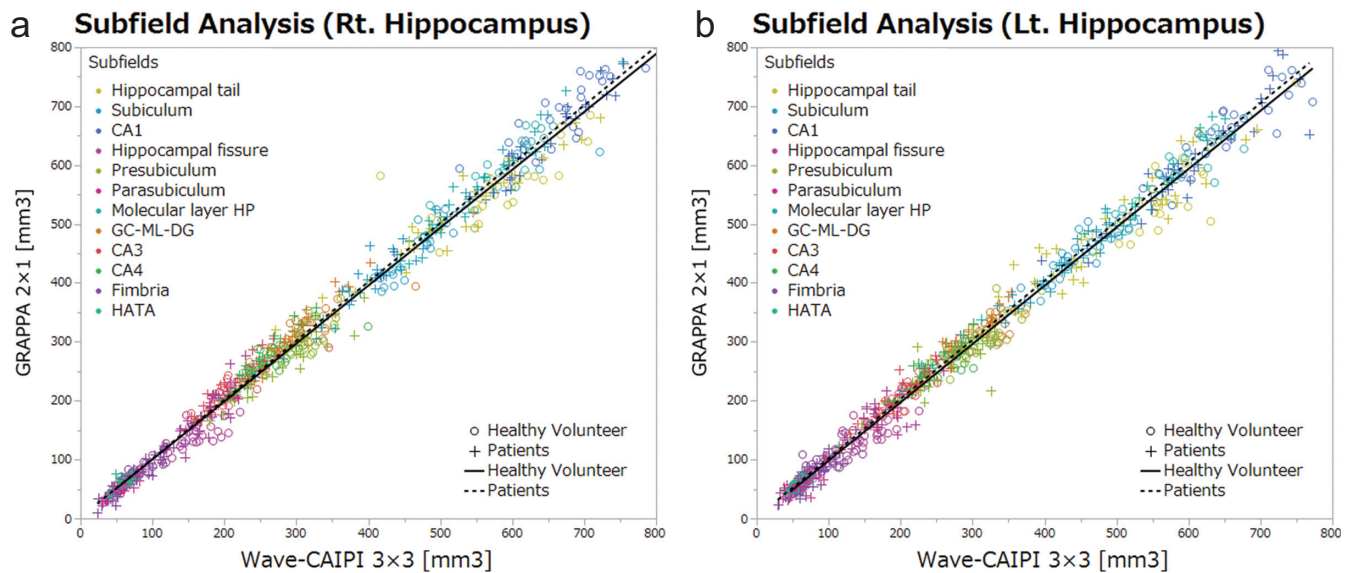
Fig. 7 The subfield analysis results of hippocampus are shown (right, **a** and left, **b**). Subfield analysis of bilateral hippocampi showed relatively higher or almost equal correlation between GRAPPA 2 × 1 and Wave-CAIPI 3 × 3. CAIPI, controlled aliasing in parallel imaging; GC-ML-DG, granule cell and molecular layer of the dentate gyrus; GRAPPA, generalized autocalibrating partially parallel acquisition; HATA, hippocampal-amygdaloid transition region; Lt., left; Rt., right.

worsened passing from mild cognitive impairment to the AD group.[36] The memory impairment was mainly associated with subfield-specific hippocampal damage in temporal lobe epilepsy with mesial temporal lobe sclerosis.[37] Our results showed good correlation of hippocampal subfields between MPRAGE GRAPPA 2×1 and Wave-CAIPI 3×3, which will lead to the short scan time protocol of volumetric studies by using Wave-CAIPI technique.

There are several limitations in this study. First, a limited number of subjects were included in this study. Healthy volunteers and patients were included in this study; however, studies with the large number of subjects are preferable for evaluation of the new technique. Second, only one software was used in this study. Volumetric methods with conventional MRI were also conducted with FMRIB Software Library (FSL; https://fsl.fmrib.ox.ac.uk/fsl/fslwiki/FSL), or statistical parametric mapping.[8,38] Synthetic MRI and deep learning technique have been used in this field.[39,40] The aim of this study was to evaluate the short scan time image sequence of Wave-CAIPI for visual and quantitative analyses; however, comparison with deep learning analysis may augment the volumetric analysis.

Conclusion

MPRAGE with Wave-CAIPI 3 × 3 has high correlation MPRAGE GRAPPA 2 × 1 in volume measurement, including hippocampal region even with 1/3 of the scan time. MPRAGE with Wave-CAIPI 3 × 3 can be applied clinically comparable to MPRAGE GRAPPA 2 × 1.

Ethical Approval

All procedures performed in the studies involving human participants were in accordance with the ethical standards of the institutional and/or national research committee and with the 1964 Helsinki Declaration and its later amendments or comparable ethical standards.

Informed Consent

This prospective study was approved by the local institutional review boards and written informed consent was obtained from patients and healthy volunteers.
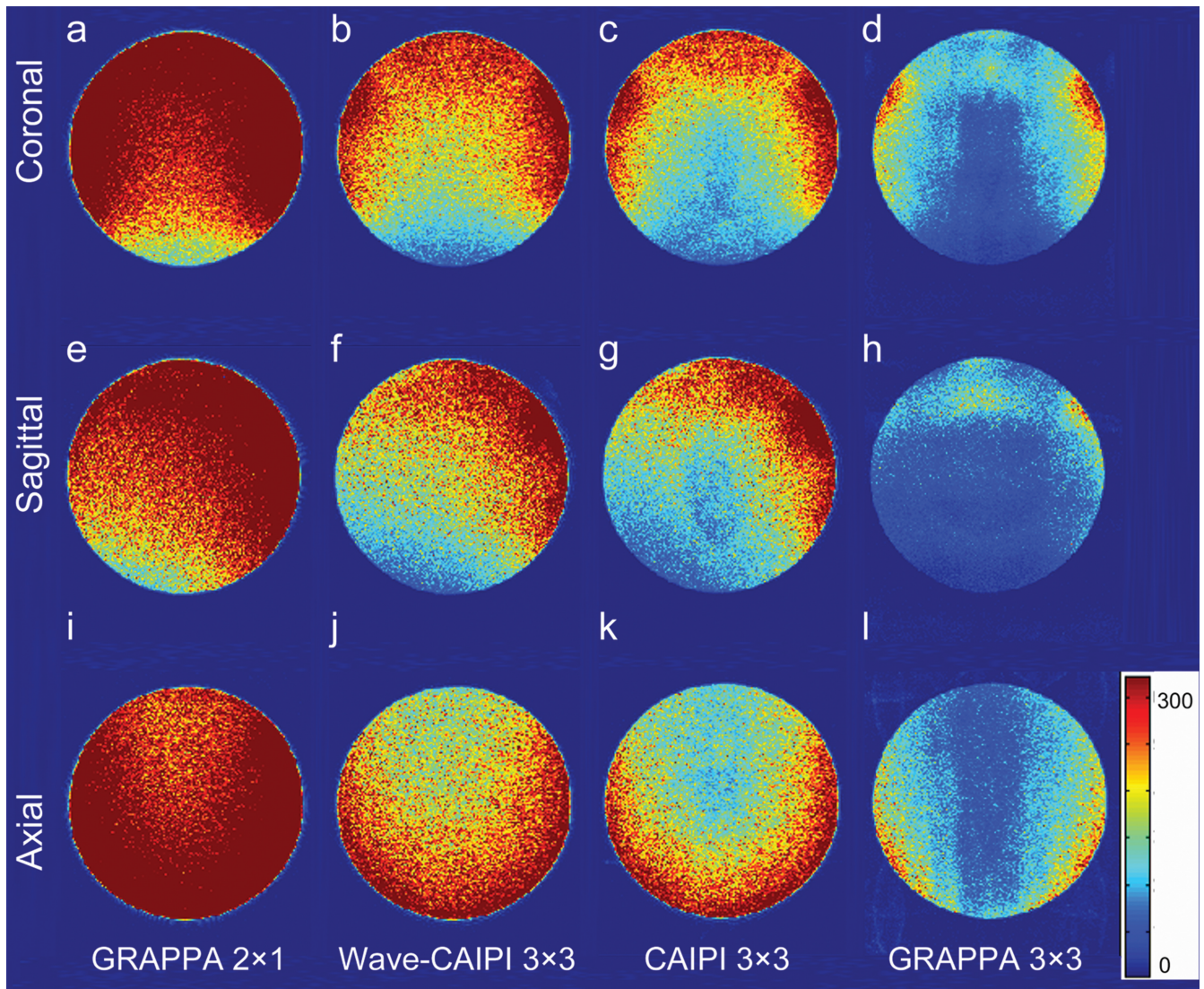
Funding

Acknowledgments

Conflicts of Interest

Wei Liu, is the employee of Siemens Shenzhen Magnetic Resonance Ltd. Tomohisa Okada received research funding received a research grant for 7 T MR from Siemens

Fig. 8 SNR maps of MPRAGE images of GRAPPA 2 × 1, Wave-CAIPI 3 × 3, CAIPI 3 × 3, and GRAPPA 3 × 3 are shown. GRAPPA 2 × 1 showed the highest SNR among the four MPRAGEs. SNR map of Wave-CAIPI 3 × 3 showed higher SNR than that of CAIPI 3 × 3 and GRAPPA 3 × 3. SNR map of CAIPI 3 × 3 showed slightly lower SNR in the center part of the FOV, and SNR map of GRAPPA 3 × 3 showed lowest SNR in the center part of FOV. CAIPI, controlled aliasing in parallel imaging; GRAPPA, generalized autocalibrating partially parallel acquisition.

Healthcare K.K. The other authors declare that they have no conflicts of interest in this study.

Supplementary Information

Supplementary files below are available online.

Supplementary Table 1
Imaging parameters of four MPRAGEs.

Supplementary Table 2
The other volume calculation results of healthy subjects are shown. Segmentation function of CAT12 with SPM12, and the LBPA40 atlas was used for volume calculation (mL).

Supplementary Fig. 1
The image noise and signal uniformity were evaluated in the center part of the images (arrows), and delineation of cortico-medullary junction at the level of putamen (arrowheads) on a 5-point scale: No image noise and excellent visualization of the corticomedullary junction (A, grade 5); less image noise in the center and clear visualization of the corticomedullary junction (B, grade 4); low image quality in the center and partly unclear visualization of the corticomedullary junction (C, grade 3); overall low image quality and unclear visualization of the corticomedullary junction (D, grade 2); and severe noise and hard to detect the corticomedullary junction (E, grade 1).

Supplementary Fig. 2
The results of recon-all function of all subjects are shown. The details of values are shown in Table 1.

Supplementary Fig. 3
The results of subfield analysis of all subjects are shown in the above figures. The details of values are shown in Table 2.

Supplementary Fig. 4
The results of recon-all function of healthy volunteers and patients are shown. The details of values are shown in Table 3.

Supplementary Fig. 5
The results of subfield analysis of healthy volunteers and patients are shown in the above figures. The details of values are shown in Table 4.

Supplementary Fig. 6
Bland-Altman analysis was performed between the measurements of GRAPPA 2×1 and Wave-CAIPI 3×3, and most of the data were distributed between 1.96 SD.

References

1. Wright IC, McGuire PK, Poline JB, et al. A voxel-based method for the statistical analysis of gray and white matter density applied to schizophrenia. Neuroimage 1995; 2:244–252.
2. Ashburner J, Friston KJ. Voxel-based morphometry—the methods. Neuroimage 2000; 11:805–821.
3. Minkova L, Habich A, Peter J, et al. Gray matter asymmetries in aging and neurodegeneration: A review and meta-analysis. Hum Brain Mapp 2017; 38:5890–5904.
4. Goto M, Hagiwara A, Fujita S, et al. Influence of mild white matter lesions on voxel-based morphometry. Magn Reson Med Sci 2021; 20:40–46.
5. Wonderlick JS, Ziegler DA, Hosseini-Varnamkhasti P, et al. Reliability of MRI-derived cortical and subcortical morphometric measures: effects of pulse sequence, voxel geometry, and parallel imaging. Neuroimage 2009; 44:1324–1333.
6. Fischl B, Dale AM. Measuring the thickness of the human cerebral cortex from magnetic resonance images. Proc Natl Acad Sci U S A 2000; 97:11050–11055.
7. Takeshita Y, Watanabe K, Kakeda S, et al. Early volume reduction of the hippocampus after whole-brain radiation therapy: an automated brain structure segmentation study. Jpn J Radiol 2020; 38:118–125.
8. Yamanakkanavar N, Choi JY, Lee B. MRI segmentation and classification of human brain using deep learning for diagnosis of alzheimer's disease: a survey. Sensors (Basel) 2020; 20:3243.
9. Peixoto-Santos JE, de Carvalho LED, Kandratavicius L, et al. Manual hippocampal subfield segmentation using high-field MRI: impact of different subfields in hippocampal volume loss of temporal lobe epilepsy patients. Front Neurol 2018; 9:927.
10. Wenger E, Mårtensson J, Noack H, et al. Comparing manual and automatic segmentation of hippocampal volumes: reliability and validity issues in younger and older brains. Hum Brain Mapp 2014; 35:4236–4248.
11. Bishop CA, Jenkinson M, Andersson J, et al. Novel fast marching for automated segmentation of the hippocampus (FMASH): method and validation on clinical data. Neuroimage 2011; 55:1009–1019.
12. Merkel B, Steward C, Vivash L, et al. Semi-automated hippocampal segmentation in people with cognitive impairment using an age appropriate template for registration. J Magn Reson Imaging 2015; 42:1631–1638.
13. Mulder ER, de Jong RA, Knol DL, et al. Alzheimer's disease neuroimaging initiative. Hippocampal volume change measurement: quantitative assessment of the reproducibility of expert manual outlining and the automated methods FreeSurfer and FIRST. Neuroimage 2014; 92:169–181.
14. Cover KS, van Schijndel RA, Bosco P, et al. Alzheimer's disease neuroimaging initiative. Can measuring hippocampal atrophy with a fully automatic method be substantially less noisy than manual segmentation over both 1 and 3 years? Psychiatry Res Neuroimaging 2018; 280:39–47.
15. Khlif MS, Werden E, Egorova N, et al. Assessment of longitudinal hippocampal atrophy in the first year after ischemic stroke using automatic segmentation techniques. Neuroimage Clin 2019; 24:102008.
16. Polak D, Setsompop K, Cauley SF, et al. Wave-CAIPI for highly accelerated MP-RAGE imaging. Magn Reson Med 2018; 79:401–406.
17. Griswold MA, Jakob PM, Heidemann RM, et al. Generalized autocalibrating partially parallel acquisitions (GRAPPA). Magn Reson Med 2002; 47:1202–1210.
18. Pruessmann KP, Weiger M, Scheidegger MB, et al. SENSE: sensitivity encoding for fast MRI. Magn Reson Med 1999; 42:952–962.
19. Breuer FA, Blaimer M, Mueller MF, et al. Controlled aliasing in volumetric parallel imaging (2D CAIPIRINHA). Magn Reson Med 2006; 55:549–556.
20. Bilgic B, Gagoski BA, Cauley SF, et al. Wave-CAIPI for highly accelerated 3D imaging. Magn Reson Med 2015; 73:2152–2162.
21. Moriguchi H, Duerk JL. Bunched phase encoding (BPE): a new fast data acquisition method in MRI. Magn Reson Med 2006; 55:633–648.
22. Breuer FA, Moriguchi H, Seiberlich N, et al. Zigzag sampling for improved parallel imaging. Magn Reson Med 2008; 60:474–478.
23. Seiberlich N, Breuer F, Blaimer M, et al. Self-calibrating GRAPPA operator gridding for radial and spiral trajectories. Magn Reson Med 2008; 59:930–935.
24. Dale AM, Fischl B, Sereno MI. Cortical surface-based analysis. I. Segmentation and surface reconstruction. Neuroimage 1999; 9:179–194.
25. Reuter M, Rosas HD, Fischl B. Highly accurate inverse consistent registration: a robust approach. Neuroimage 2010; 53:1181–1196.
26. Polak D, Cauley S, Huang SY, et al. Highly-accelerated volumetric brain examination using optimized wave-CAIPI encoding. J Magn Reson Imaging 2019; 50:961–974.
27. Polak D, Chatnuntawech I, Yoon J, et al. Nonlinear dipole inversion (NDI) enables robust quantitative susceptibility mapping (QSM). NMR Biomed 2020; 33:e4271.
28. Conklin J, Longo MGF, Cauley SF, et al. Validation of highly accelerated wave-CAIPI SWI compared with conventional SWI and T2*-weighted gradient recalled-echo for routine clinical brain MRI at 3T. AJNR Am J Neuroradiol 2019; 40:2073–2080.

29. Chung MS, Lee EJ, Kim S, et al. Wave-CAIPI susceptibility-weighted imaging achieves diagnostic performance comparable to conventional susceptibility-weighted imaging in half the scan time. Eur Radiol 2020; 30:2182–2190.

30. Longo MGF, Conklin J, Cauley SF, et al. Evaluation of ultrafast wave-CAIPI MPRAGE for visual grading and automated measurement of brain tissue volume. AJNR Am J Neuroradiol 2020; 41:1388–1396.

31. Fischl B, Salat DH, Busa E, et al. Whole brain segmentation: automated labeling of neuroanatomical structures in the human brain. Neuron 2002; 33:341–355.

32. Iglesias JE, Augustinack JC, Nguyen K, et al. Alzheimer's disease neuroimaging initiative. A computational atlas of the hippocampal formation using ex vivo, ultra-high resolution MRI: Application to adaptive segmentation of in vivo MRI. Neuroimage 2015; 115:117–137.

33. Gaser C, Dahnke R. CAT-A Computational anatomy toolbox for the analysis of structural MRI data. Proceedings of 22nd annual meeting of the organization for human brain mapping, Geneva, 2016; 4057.

34. Shattuck DW, Mirza M, Adisetiyo V, et al. Construction of a 3D probabilistic atlas of human cortical structures. Neuroimage 2008; 39:1064–1080.

35. Rössler M, Zarski R, Bohl J, et al. Stage-dependent and sector-specific neuronal loss in hippocampus during alzheimer's disease. Acta Neuropathol 2002; 103:363–369.

36. Carlesimo GA, Piras F, Orfei MD, et al. Atrophy of presubiculum and subiculum is the earliest hippocampal anatomical marker of alzheimer's disease. Alzheimers Dement (Amst) 2015; 1:24–32.

37. Mueller SG, Laxer KD, Scanlon C, et al. Different structural correlates for verbal memory impairment in temporal lobe epilepsy with and without mesial temporal lobe sclerosis. Hum Brain Mapp 2012; 33:489–499.

38. Wachinger C, Reuter M, Klein T. DeepNAT: deep convolutional neural network for segmenting neuroanatomy. Neuroimage 2018; 170:434–445.

39. Hagiwara A, Warntjes M, Hori M, et al. SyMRI of the brain: rapid quantification of relaxation rates and proton density, with synthetic MRI, automatic brain segmentation, and myelin measurement. Invest Radiol 2017; 52:647–657.

40. Granberg T, Uppman M, Hashim F, et al. Clinical feasibility of synthetic MRI in multiple sclerosis: a diagnostic and volumetric validation study. AJNR Am J Neuroradiol 2016; 37:1023–1029.